

Tuning the Work-Function Via Strong Coupling

James A. Hutchison, Andrea Liscio, Tal Schwartz, Antoine Canaguier-Durand, Cytiaque Genet, Vincenzo Palermo, Paolo Samori, and Thomas W. Ebbesen*

All materials are characterized by a work-function, the energy necessary to remove an electron from the Fermi level into vacuum, which is a fundamental property critical for many applications.^[1,2] Electronic devices, such as organic transistors and solar cells, are designed with sets of metal electrodes carefully chosen according to their intrinsic work-function.^[3–7] The work-function can be further adjusted by chemical modification of the interfaces to optimize the performance of such devices.^[7–11] Here we demonstrate that the work-function can also be modified by engineering the electromagnetic environment of the material. To do this, we create hybrid light-matter states that strongly change the electronic energy levels of the system as explained next.

Through the rapid exchange of photons, matter can enter into the so-called strong coupling regime with the surrounding electromagnetic field. This leads to the formation of two new eigenstates, $|P - \rangle$ and $|P + \rangle$, separated by the Rabi splitting energy as illustrated in **Figure 1A** and **B**. To achieve this regime, the material is typically placed in a photonic structure or an optical cavity that is resonant with one of its electronic transitions. A prerequisite for strong coupling is that the photon exchange must be faster than any dissipation process, which is facilitated by shaping the electromagnetic environment and confining the field. Strong coupling has been extensively studied with atoms, semi-conductors and quantum wells as it offers much potential in areas such as Bose-Einstein type condensation of polaritons, spintronics, lasing and quantum information processing.^[12–18] Nevertheless the potential of strong coupling is not limited to such physics applications. One of the fascinating features of strong coupling for material and molecular science is its collective nature.^[19] In a strongly coupled molecular material, the Rabi-splitting is determined by the square root of the molecular concentration within the optical mode, and molecules microns apart will emit coherently if they are strongly coupled to the same mode.^[20] Another important feature is the fact that strong coupling occurs even in the absence of light: according to quantum mechanics, the Rabi-splitting energy $\hbar\Omega_R$ is given, neglecting dissipation, by

$$\hbar\Omega_R = 2\sqrt{\frac{\hbar\omega}{2\varepsilon_0\nu}} \cdot d \cdot \sqrt{n_{ph} + 1} \quad (1)$$

where $\hbar\omega$ is the cavity resonance or transition energy, ε_0 the vacuum permittivity, ν the mode volume, d the transition dipole moment of the material and n_{ph} the number of photons present in the system. Even when n_{ph} goes to zero, $\hbar\Omega_R$ has a finite value. This implies that even in the dark, the interaction of the material with the vacuum field via the photonic structure can be very strong, and we have recently demonstrated a vacuum Rabi splitting of 700 meV.^[21] Such high values lead to a major reorganization of the energy levels of the system and as a consequence, chemical reactivity of molecules coupled to the vacuum field can be modified, as shown recently.^[22] Other properties might also be changed. For instance it is well known that the ionisation potential and the electronic affinity of first excited state can be estimated from the electronic energies of highest occupied orbital (HOMO) and the lowest unoccupied orbital (LUMO) of the ground state and the transition energy between the two states.^[23,24] With this in mind, one might expect that the formation of the new hybrid states modify similarly the electronic energies of the system.

To check if this is the case or not, we have explored whether strong coupling can be used to modify the work-function (Φ). The work-function is the energy difference between the Fermi level of a material and the vacuum energy level. For a semi-conductor, or an insulating material, the Fermi level lies in the bandgap between the HOMO and the LUMO of the material.^[1,2] In general, the work function of a semi-conductor can be written as $\Phi_{sample} = E^a + \Delta E_{fn}$, where ΔE_{fn} is the Fermi level position referenced to the bottom of the conduction band and E^a is the electron affinity. Changes in work-function for organic materials are routinely measured by the Kelvin Probe Method (KPM).^[7–11,25,26]

KPM measures the surface potential difference (ΔSP) between a metal tip and a sample, as schematically illustrated in **Figure 1F**. For a metallic sample, ΔSP relates directly to the difference in work-functions ($\Delta\Phi$) between the tip and sample. In the case of semi-conductors and insulators, there can also be a contribution from charges distribution in the material and surface dipoles (collectively denoted μ) and from electronic arrangement at the film/substrate interface (δ):

$$\Delta SP = \Delta\Phi + \mu + \delta \quad (2)$$

As we will show here, the change in surface potential recorded upon strong coupling in the following experiments can only be attributed to a change in $\Delta\Phi$.

For this purpose, a polymer film heavily doped (50% by weight, density $\sim 10^{20} \text{ cm}^{-3}$) with the photochrome spiropyran

Dr. J. A. Hutchison, Dr. T. Schwartz,
Dr. A. Canaguier-Durand, Dr. C. Genet,
Prof. P. Samori, Prof. T. W. Ebbesen
ISIS & icFRC, Université de Strasbourg and CNRS
8 allée Gaspard Monge, Strasbourg, 67000, France
E-mail: ebbesen@unistra.fr

Dr. A. Liscio, Dr. V. Palermo
Istituto per la Sintesi e la Fotoreattività
CNR, via Gobetti 101, Bologna, 40120, Italy



DOI: 10.1002/adma.201203682

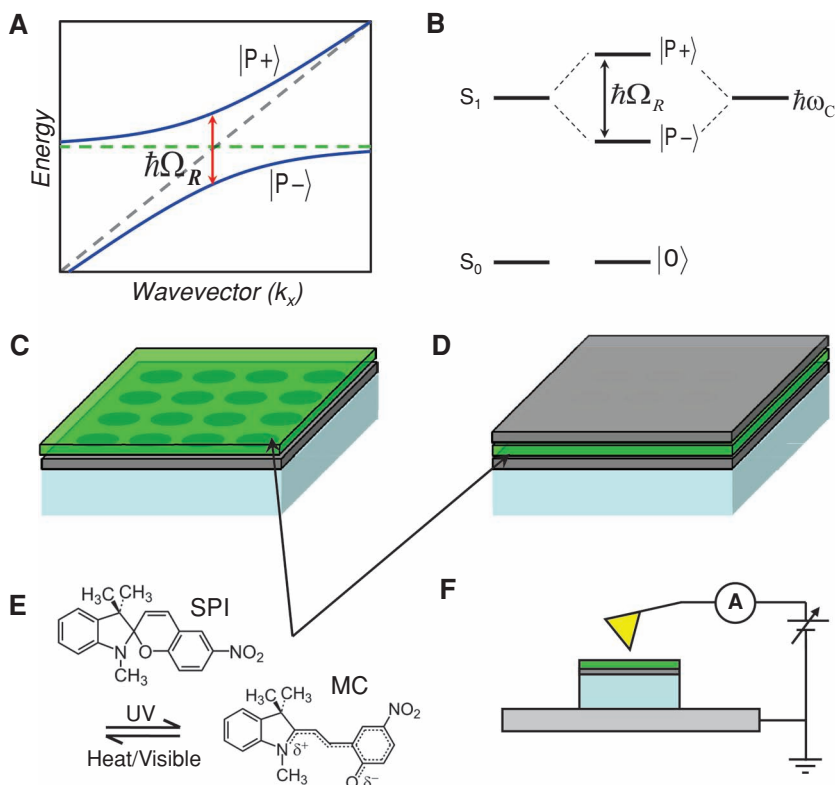


Figure 1. A) Dispersion diagram of strong coupling between a dispersive optical mode (dark dashed line) and a non-dispersive electronic transition (green dashed line) resulting in the anti-crossing with a Rabi splitting $\hbar\Omega_R$ between the lower $|P-\rangle$ and upper $|P+\rangle$ polaritonic states (blue lines). B) Diagram of the modification of a molecular material's energy levels upon strong coupling (molecular ground state S_0 and first excited state S_1). C) Schematic of a hole array milled in Ag film on a glass substrate with spin-cast polymer layer on top which contains the photochrome. D) Schematic of a Fabry-Perot cavity formed by two Ag mirrors on either side of the polymer film containing the photochrome, all of it on a glass substrate. E) Photochrome in its two isomeric structures, the uncoloured spiropyran (SPI) form and the coloured merocyanine form (MC). F) A schematic diagram of the Kelvin probe force microscope use to measure the work-function.

(SPI) was chosen. The SPI form of the photochrome can be photoisomerized to the coloured merocyanine (MC) (Figure 1E). We have previously established that the first transition (560 nm) of MC, corresponding to the HOMO-LUMO transition, can be strongly coupled with the optical cavities leading to exceptionally large vacuum Rabi splittings.^[21] Furthermore the degree of coupling can be adjusted by UV irradiation of SPI to control [MC] and thereby $\hbar\Omega_R$ since it is proportional to $\sqrt{[MC]}$. As we will see, this ability to reversibly control the degree of strong coupling *in situ* in this material is crucial to extracting the effect of strong coupling on the work-function of a material.

Two types of resonant photonic structures were tested, one a plasmonic hole array and the other a Fabry-Perot micro-cavity as shown in Figure 1C and 1D. The experiments using plasmonic hole arrays will be discussed first. As described in detail in the Experimental section, a series of hole arrays with different periods were milled using focused ion beam (FIB) in a 200 nm thick Ag film. A 130 nm thick film of the material was then spin-coated on the surface. A topographical AFM image of a 250 nm period hole array with the polymer layer is shown

in Figure 2A. Transmission spectra of the arrays were recorded by optical microscopy which showed the typical extraordinary transmission peaks associated with the surface plasmon modes (black curve, Figure 2C).^[27,28] The sample was then irradiated at 365 nm to generate MC. When the (1,0) surface plasmon mode was resonant with the 560 nm MC peak (period, $P = 250$ nm), a splitting occurs which here reaches a maximum of 600 meV, a typical signature of strong coupling (red curve, Figure 2C). As the period increases and the surface plasmon mode is detuned from the MC transition, the strong coupling vanishes.^[21,27] This is shown in Figure 2D where the energies of the transmission maxima are plotted as a function of $2\pi \cdot \text{Period}^{-1}$ of the different samples.

The surface potential difference ΔSP was then measured for the same set of arrays *before* and *after* UV irradiation. The samples before irradiation with the SPI isomer acted as a reference. For fabrication reasons, the size of the nanostructured arrays are limited to ca. $10 \mu\text{m} \times 10 \mu\text{m}$ in area, and thus Kelvin Probe Force Microscopy (KPFM, see Experimental section) was used to extract ΔSP due to its high spatial resolution.^[25,26]

An example of a KPFM surface potential map of a hole array is shown in Figure 2B. As the surface area of the sample interacting with the probe (ca. 200–300 nm) is similar to the period and hole diameter range, it is difficult to distinguish ΔSP in and out of holes. Rather ΔSP for each array was calculated as an average value over a $5 \mu\text{m} \times 5 \mu\text{m}$ region in the centre of the array (thus avoiding edge effects), and importantly also from an area of flat metal nearby (indicated by the red

squares in Figure 2B).

The shift in ΔSP (*i.e.* upon switching from spiropyran to merocyanine by UV irradiation, $\Delta SP_{MC} - \Delta SP_{SPI}$) measured on the flat Ag film is -155 ± 7 mV (see black squares Figure 2E). However, when the same comparison is done on the hole arrays, the shift in ΔSP reaches a maximum ($\Delta SP_{MC} - \Delta SP_{SPI} = -275$ mV) when the surface plasmon mode is resonant with the MC transition (period 250 nm), *i.e.* when the system is most strongly coupled as confirmed by optical methods (compare Figure 2D and 2E).

The change in ΔSP due to photoisomerisation of spiropyran to merocyanine diminishes upon detuning of the resonance of the hole array, approaching that of the flat film at large periods. This is an important result which we will return to further on. The maximum change in ΔSP between the flat film and the strongly coupled samples (-120 ± 10 mV at period 250 nm) is an underestimate because the surface plasmon modes of the hole array have strong angular dispersion^[27,28] (as illustrated in Figure 1A and visible in Figure 2D and E) and the KPFM probe, with its sharp tip, averages over a large solid angle, thereby

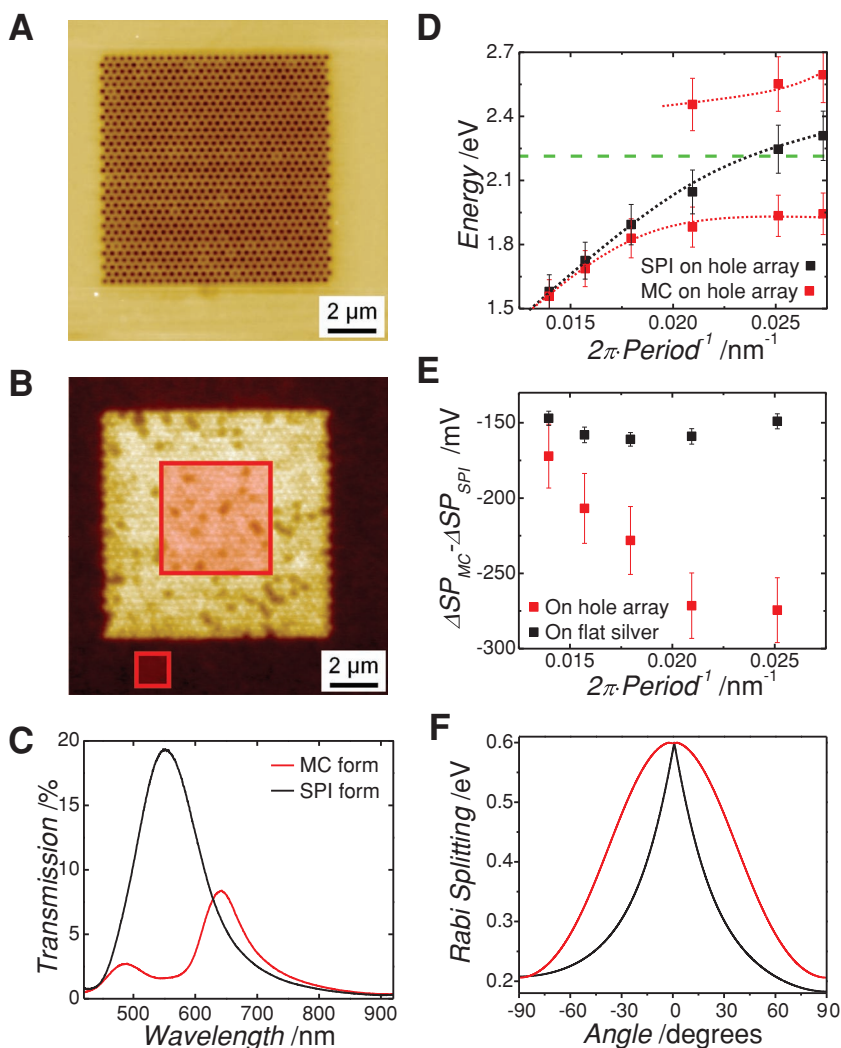


Figure 2. A) AFM image (Z-range 100 nm) of a hole array sample (period 250 nm, with 130 nm thick PMMA film containing SPI). B) KPFM image of the same sample as in (A) (Z-range 200 mV). C) Transmission spectra of a hole array (period 250 nm) acquired (black) before and (red) after the photoisomerisation of SPI to MC. D) Dispersion curve of hole array as recorded for different array periods with SPI (black) and MC (red), the absorption peak of MC indicated by green dashed line. E) The shift in ΔSP induced by the conversion of SPI to MC measured with KPFM inside (red) and outside the hole array (black) as a function of array period, plotted as $2\pi \cdot \text{Period}^{-1}$. The areas over which the different measurements were averaged are shown by the red boxes in Figure 2B. F) Predicted angular dependence for the Rabi splitting in the cases of a plasmonic array (black curve) and of a Fabry-Perot cavity (red curve), both being at resonance for normal incidence. The corresponding equations are given in the experimental section.

blurring the true value of ΔSP . That is why even at off-resonance periods a slight difference remains as compared to the measurements on the flat metal substrate. Indeed, as can be seen in Figure 2F, showing the predicted change in Rabi splitting with observation angle for a plasmonic array (black curve), the magnitude of the coupling depends strongly on the incidence angle, and the contribution of non-zero angles will thus lead to a severe averaging of the effect of strong coupling.

In order to approach the absolute value for the shift in ΔSP due to strong coupling, Fabry-Perot (FP) structures were prepared as these cavities have much smaller angular dispersion

(see also Figure 2F, red curve). In addition, the FP cavities can be made over a large area (ca. 30 mm²) which allowed us to do macroscopic Kelvin Probe^[29] measurements using a much bigger probe (2 mm diameter) thereby reducing significantly the contributions from angles other than those normal to the FP surface. The FP cavities were prepared such that the MC transition (560 nm) was strongly coupled to the λ mode, as shown spectroscopically in Figure 3A. The corresponding Rabi splitting is 670 meV. Great care was taken that there was no electrical contact between the two mirrors (see Experimental section) to ensure that the true change in ΔSP was detected by the Kelvin probe.

Upon UV irradiation of the resonant FP cavity, and in keeping with the measurements for the hole arrays, ΔSP shifts negatively with time as merocyanine concentration builds up and strong coupling conditions are reached (black curve, Figure 3B, note the initial ΔSP for the FP cavity measurements are normalised to 0 V in Figure 3B to emphasize the comparative shifts occurring upon irradiation). The maximum observed change is indeed much larger for the resonant FP cavity (−175 mV) compared to a resonant hole array (−120 mV). The shift in ΔSP could be completely reversed by irradiating the sample with visible light, i.e. by switching the photochrome back to the spiropyran form (Figure 3B).

As a control, a FP cavity of the same thickness but with only the PMMA polymer showed no measurable shift in ΔSP upon irradiation (green curve, Figure 3B). A more important control is the off-resonance FP cavity which consists of the SPI doped PMMA layer of a thickness such that the cavity resonance is detuned (to 460 nm) from the MC absorption and thus cannot result in strong coupling. Upon irradiation and the formation of MC, the measured ΔSP for the off-resonance sample shifts positively by a few tens of mV (red curve, Figure 3B).

The total change in ΔSP for on (ΔSP_{on}) and off-resonance (ΔSP_{off}) FP cavities containing the maximum (photostationary) concentration of merocyanine is therefore $\Delta SP_{on} - \Delta SP_{off} \approx -200 \pm 20$ mV. As mentioned already, ΔSP contains contributions not only from work-function but also from charge/dipole effects (Equation 2) and therefore the changes can be written as follows:^[5,30,31]

$$\Delta SP_{on} - \Delta SP_{off} = (\Delta\Phi_{on} + \mu_{on} + \delta_{on}) - (\Delta\Phi_{off} + \mu_{off} + \delta_{off}) \quad (3)$$

If there is no realignment of molecules in the sample due to strong coupling, both the μ and δ terms will make the same

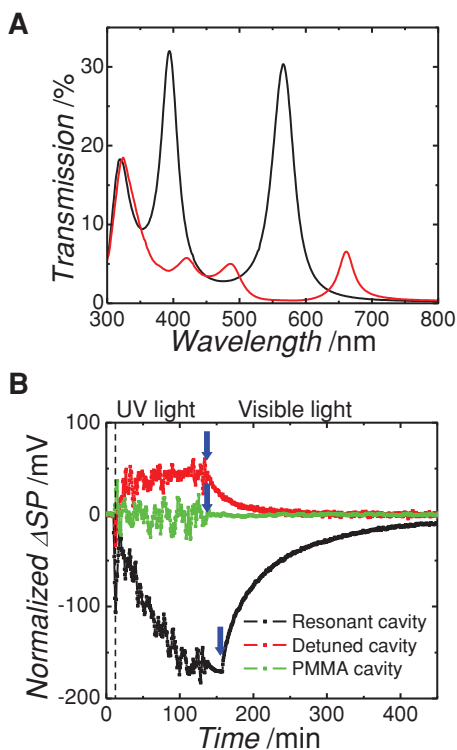


Figure 3. A) Transmission spectra of the Fabry-Perot cavity before (black) and after (red) photoisomerisation of SPI to MC. Notice the split peak (new peaks at 490 and 660 nm) due to strong coupling. B) Evolution of the observed ΔSP (normalized to zero at the initial measurement) as a function of UV irradiation time (onset indicated by black dashed line) and then visible light once the photostationary state was reached (onset indicated by blue arrows), for the resonant cavity (black), the detuned cavity (red) and for the resonant cavity without photochrome (green).

contributions the measurements on and off resonance and $\Delta SP_{on} - \Delta SP_{off} = \Delta \Phi_n - \Delta \Phi_{off} = \Delta \Phi_{SC}$. In other words, the change in ΔSP reflects only the absolute change in work-function $\Delta \Phi_{SC}$ due to strong coupling. Nevertheless the possibility of realignment of molecules by strong interaction with the vacuum field is real since coupling is favoured for a specific dipole orientation relative to the field. This would actually be a very important finding. In order to check for such a possibility we carried out two experiments.

In the first experiment, we confirmed that strong coupling did not favour a given orientation during the conversion of SPI to MC. A FP cavity was constructed in which conversion from SPI to MC by UV irradiation was accomplished prior to sputtering the top Ag layer. Optical measurements showed that Rabi splitting of 650 meV was achieved with this sample. We then measured ΔSP on this sample before and after application of visible light (to switch MC back to SPI) and observed the same shift in ΔSP (within experimental error, ca. ± 20 mV) as for the samples where MC was generated inside the cavity.

In the second experiment, we looked for light polarisation anisotropy that would be associated with molecular alignment by comparing MC films photo-generated outside a cavity or inside a resonant cavity under strong coupling conditions. No difference in anisotropy could be observed.

We can therefore conclude from all the above experiments that the measured change in ΔSP induced by strong coupling is due to a change in work-function of the material. It demonstrates that the splitting of the excited state into $|P+\rangle$ and $|P-\rangle$ does indeed affect the electronic energy levels. As a consequence, it will impact all redox processes.

The work-function modification induced by strong coupling is smaller than that achievable by chemical means.^[7–11] Nevertheless it has the advantage that it can be easily fine-tuned to a desired value which is naturally critical for many applications. This is especially true for organic devices such as transistors, light-emitting devices and solar cells. It can also be dynamically controlled by using functional molecules such as photochromes and electrochromes. Alternatively, the strong coupling could be modulated using MEMS technology to control the cavity resonance. For instance, the distance between two metallic electrodes or dielectric mirrors in a sandwich structure could be adjusted to resonate with an electronic transition in the material. Tuning of the work-function through strong coupling should be quite easy to implement in practice.

It is interesting to note that hybridization with the vacuum field introduces a dispersive character to the work-function as seen in Figure 2E. Plasmonic resonances could be used either with non-dispersive localized modes or delocalized ones as illustrated in this work. Finally, this first non-optical observation of strong coupling provides evidence that strongly coupled materials are fundamentally modified even in the absence of light by the formation of new hybrid states. This further confirms the potential of strong coupling for materials engineering and device design.

Experimental Section

Kelvin Probe techniques: Both macroscopic Kelvin probe (KP) and Kelvin probe force microscopy (KPFM) techniques use a metallic tip vibrating at fixed frequency, while the sample placed on a conducting support is grounded. For KP, a steady AC current develops in the tip-sample capacitor. For KPFM, which is based on an AFM setup, electrostatic tip-sample interactions are measured by detecting the tip oscillation amplitude. An additional DC bias is then applied between the electrodes to nullify either the AC current for KP or the electrostatic forces for KPFM. KP measurements were performed under ambient conditions using a 2 mm diameter gold tip amplifier (Ambient Kelvin Probe Package from KP Technology Ltd.). KPFM measurements were carried out with a commercial microscope Multimode (Bruker) with Extender Electronics module. In order to obtain a sufficiently large and detectable mechanical deflection, we used ($k = 2.8 \text{ N m}^{-1}$) Pt/Ir coated Si ultra levers (SCM, Bruker) with oscillating frequencies in the range 60 to 90 KHz. AFM and KPFM images are acquired in the same measurement; a topographic line scan is first obtained by AFM operating in Tapping Mode and then that same line is rescanned in Lift Mode with the tip raised to a lift height of 10 nm. KPFM measurements were performed in a home-made, sealed chamber with relative humidity (<5%) maintained by blowing a gentle flow of N_2 . Both techniques provide a voltage resolution of about 5 mV, while the lateral resolution is a few millimeters or a few tens of nanometers for KP and KPFM, respectively. Calibration of the probe was performed against a freshly cleaved High Oriented Pyrolytic Graphite surface for both techniques. A comprehensive description of the two techniques can be found in refs. [26] and [32], and references therein. In order to check the stability of the sample due to the UV degradation, KP and KPFM measurements were performed on the same samples repeating the light/dark cycle for three times to obtain the complete and reversible photoisomerisation of the samples.

Sample Preparation: Plasmonic hole arrays were prepared by e-beam evaporation of 200 nm of Ag on glass substrates and milling periodic hole arrays in hexagonal symmetry using FIB. A toluene solution of SPI and PMMA (both 1% by weight) was spin-cast on the samples to yield a dry film of thickness ca. 130 nm. Fabry-Perot cavities were prepared by first sputtering 30 nm Ag on a cleaned glass substrate. Then 1% by weight PDMS (polydimethylsiloxane, hydroxyl-terminated, MW = 110 000, Aldrich) dissolved in tertiary butanol was spin-cast at ca. 4000 rpm on the sample to afford a ca. 30 nm thick layer which was exposed to UV/Ozonolysis for hardening purposes. This layer ensured the electrical isolation of the bottom Ag mirror. The same SPI/PMMA solution was then spin-cast on top of the oxidized PDMS to yield a total thickness of 260 nm before sputtering the top 30 nm Ag mirror. The photoisomerisation of SPI to MC was achieved with a UV pen lamp until the photostationary state was reached.

Calculations: The change in the Rabi-splitting energy $\hbar\Omega_R$ caused by the incidence angle θ was estimated for a plasmonic hole array and for a Fabry-Perot micro-cavity. For the former case, the incident angle θ determines the matching wave-vector condition that the (1,0) surface plasmon mode must verify according to the following equation:

$$\frac{\omega}{c} \operatorname{Re} \left(\sqrt{\frac{\varepsilon_d \varepsilon_m}{\varepsilon_d + \varepsilon_m}} \right) = \frac{n\omega}{c} \sin(\theta) + \frac{2}{\sqrt{3}} \frac{2\pi}{P} \quad (4)$$

where c is the speed of light, n the refractive index, ε_d and ε_m the dielectric constants respectively for the dielectric and the metal at the frequency ω , and P the period. As the hole array is set to be resonant with the MC peak at normal incidence ($\theta = 0$), the structure becomes detuned for non-zero angles, which yields a decrease of the Rabi-splitting energy $\hbar\Omega_R$, presented by the black curve in Figure 2F. For the latter case of a micro-cavity, the energy of the structure also depends on the incidence angle θ :

$$E_{cav}(\theta) = E_{cav}(0) \times \left[1 - \left(\frac{n_{ext}}{n_{cav}} \sin \theta \right)^2 \right]^{-1/2} \quad (5)$$

where n_{ext} and n_{cav} are the refractive indices inside and outside the cavity. The structure being also resonant for normal incidence ($\theta = 0$), this also leads to a decrease of the Rabi-splitting energy $\hbar\Omega_R$ for non-zero angles, illustrated by the red curve in Figure 2F.

Acknowledgements

This work was supported by the ERC through the projects Plasmonics (GA-227557) and Suprafuction (GA-257305), the International Center for Frontier Research in Chemistry (icFRC, Strasbourg) and the European Science Foundation (ESF) under the EUROCORES Program EuroGRAPHENE (GOSPEL).

Received: September 4, 2012

Revised: January 11, 2013

Published online: March 6, 2013

- [1] S. Sze, *Physics of Semiconductor Devices*, 2nd Ed., Wiley-VCH, Weinheim, Germany **1981**.
- [2] W. R. Salaneck, S. Stafström, J.-L. Brédas, *Conjugated Polymer Surfaces and Interfaces*, Cambridge University Press, Cambridge, UK **1996**.
- [3] Y. Yuan, T. J. Reece, P. Sharma, S. Poddar, S. Ducharme, A. Gruverman, Y. Yang, J. Huang, *Nat. Mater.* **2011**, *10*, 296.

- [4] E. J. Meijer, D. M. De Leeuw, S. Setayesh, E. van Veenendaal, B.-H. Huisman, P. W. M. Blom, J. C. Hummelen, U. Scherf, T. M. Klapwijk, *Nat. Mater.* **2003**, *2*, 678.
- [5] K. Vandewal, K. Tvingstedt, A. Gadisa, O. Inganäs, J. V. Manca, *Nat. Mater.* **2009**, *8*, 904.
- [6] Y. Liang, Z. Xu, J. Xia, S.-T. Tsai, Y. Wu, G. Li, C. Ray, L. Yu, *Adv. Mater.* **2010**, *22*, E135.
- [7] H. Ishii, K. Sugiyama, E. Ito, K. Seki, *Adv. Mater.* **1999**, *11*, 605.
- [8] T. van Woudenberg, P. W. M. Blom, J. N. Huiberts, *Appl. Phys. Lett.* **2003**, *82*, 985.
- [9] B. de Boer, A. Hadipour, M. M. Mandoc, T. van Woudenberg, P. W. M. Blom, *Adv. Mater.* **2005**, *17*, 621.
- [10] S. Duhm, G. Heimel, I. Salzmann, H. Glowatzki, R. L. Johnson, A. Vollmer, J. P. Rabe, N. Koch, *Nat. Mater.* **2008**, *7*, 326.
- [11] Y. Zhou, C. Fuentes-Hernandez, J. Shim, J. Meyer, A. J. Giordano, H. Li, P. Winget, T. Papadopolous, H. Cheun, J. Kim, M. Fenoll, A. Dindar, W. Haske, E. Najafabadi, T. M. Kahn, H. Sojoudi, S. Barlow, S. Graham, J.-L. Brédas, S. R. Marder, A. Kahn, B. Kippelen, *Science* **2012**, *336*, 327.
- [12] D. Snoke, P. Littlewood, *Phys. Today* **2010**, *63*, 42.
- [13] J. Kasprzak, M. Richard, S. Kundermann, A. Baas, P. Jeambrun, J. M. J. Keeling, F. M. Marchetti, M. H. Szymanska, R. André, J. L. Staehli, V. Savona, P. B. Littlewood, B. Deveaud, L. S. Dang, *Nature* **2006**, *443*, 409.
- [14] T. K. Paraiso, M. Wouters, Y. Léger, F. Morier-Genoud, B. Deveaud-Plédran, *Nat. Mater.* **2010**, *9*, 655.
- [15] P. V. Kelkar, V. G. Kozlov, A. V. Nurmikko, C.-C. Chu, J. Han, R. L. Gunshor, *Phys. Rev. B* **1997**, *56*, 7564.
- [16] M. Saba, C. Ciuti, J. Bloch, V. Thierry-Mieg, R. André, L. S. Dang, S. Kundermann, A. Mura, G. Bongiovanni, J. L. Staehli, B. Deveaud, *Nature* **2001**, *414*, 731.
- [17] T. H. Stievater, X. Li, D. G. Steel, D. Gammon, D. S. Katzer, D. Park, C. Piermarocchi, L. J. Sham, *Phys. Rev. Lett.* **2001**, *87*, 133603.
- [18] J. M. Raimond, M. Brune, S. Haroche, *Rev. Mod. Phys.* **2001**, *73*, 565.
- [19] A. Fontcuberta i Morral, F. Stellaci, *Nat. Mater.* **2012**, *11*, 272.
- [20] S. Abeera Guebrou, C. Symonds, E. Homeyer, J. C. Plenat, Y. N. Gartstein, V. M. Agranovitch, J. Bellessa, *Phys. Rev. Lett.* **2012**, *108*, 066401.
- [21] T. Schwartz, J. A. Hutchison, C. Genet, T. W. Ebbesen, *Phys. Rev. Lett.* **2011**, *106*, 196405.
- [22] J. A. Hutchison, T. Schwartz, C. Genet, E. Devaux, T. W. Ebbesen, *Angew. Chem. Int. Ed.* **2012**, *51*, 1592.
- [23] N. J. Turro, *Modern Molecular Photochemistry*, University Science Books, Sausalito, California, USA **1991**, Ch. 2.
- [24] L. Novotny, B. Hecht, *Principles of Nano-Optics*, Cambridge University Press, Cambridge, UK **2006**, Ch. 9.
- [25] M. Nonnenmacher, M. P. O'Boyle, H. K. Wickramasinghe, *Appl. Phys. Lett.* **1991**, *58*, 2921.
- [26] A. Liscio, V. Palermo, P. Samorì, *Acc. Chem. Res.* **2010**, *43*, 541.
- [27] T. W. Ebbesen, H. J. Lezec, H. F. Ghaemi, T. Thio, P. A. Wolff, *Nature* **1998**, *391*, 667.
- [28] J. Dintinger, S. Klein, F. Bustos, W. L. Barnes, T. W. Ebbesen, *Phys. Rev. B* **2005**, *71*, 035424.
- [29] W. A. Zisman, *Rev. Sci. Instrum.* **1932**, *3*, 367.
- [30] Y. Shen, D. M. Barnett, P. M. Pinsky, *Rev. Sci. Instrum.* **2008**, *79*, 023711.
- [31] S. V. Kalinin, D. A. Bonnell, *Phys. Rev. B* **2001**, *63*, 125411.
- [32] I. D. Baikie, S. Mackenzie, P. J. Z. Estrup, J. A. Meyer, *Rev. Sci. Instrum.* **1991**, *62*, 1326.